Since January 2020 Elsevier has created a COVID-19 resource centre with free information in English and Mandarin on the novel coronavirus COVID-19. The COVID-19 resource centre is hosted on Elsevier Connect, the company's public news and information website.

Journal of Molecular Structure 1232 (2021) 130076

Contents lists available at ScienceDirect

Journal of Molecular Structure

journal homepage: www.elsevier.com/locate/molstr

Computational search for drug repurposing to identify potential inhibitors against SARS-COV-2 using Molecular Docking, QTAIM and IQA methods in viral Spike protein – Human ACE2 interface

Sergio H.D.M. Faria[a,b,*], João G. Teleschi[b]

[a] Departamento de Química e Física Molecular, Instituto de Química de São Carlos, Universidade de São Paulo, Avenida Trabalhador São-Carlense, 400, São Carlos, SP, 13560-970 Brazil
[b] Universidade Paulista, Av. Comendador Enzo Ferrari, 280–Swift, Campinas, SP, 13045-770, Brazil

ARTICLE INFO

Article history:
Received 4 January 2021
Revised 2 February 2021
Accepted 3 February 2021
Available online 8 February 2021

ABSTRACT

With the advancement of the Covid-19 pandemic, this work aims to find molecules that can inhibit the attraction between the Spike proteins of the SARS-COV-2 virus and human ACE2. The results of molecular docking positioned four molecules at the interaction site Tyr-491(Spike)-Glu-37(ACE2) and one at the site Gly-488(Spike)-Lys-353(ACE2). The QTAIM and IQA data showed that the 1629 molecule had a significant inhibitory effect on the Gly488-Ly353 site, decreasing the Laplacian of the electronic density of the BCP O_4-N_{10}. The molecule 2542 showed an inhibitory effect in two regions of interaction of the Tyr491-Glu37 site, acting on the BCPs H_{30}-H_{33} and O_8-H_{31} while the ligand 2600, in conformation 26, presented a similar effect only on the BCP O_8-H_{31} of that same interactive site. Thus, the data suggest laboratory tests of a combination of molecules that can act at two sites of interaction simultaneously, using the combination of 1629/2542 and 1629/2600 ligands.

1. Introduction

In December 2019, a new and mysterious pneumonia-related illness was reported in the city of Wuhan, located in Hubei province, China [1]. Chinese scientists quickly isolated the pathogen responsible for the disease and discovered that it was a new coronavirus belonging to the same family of viruses known as Severe Acute Respiratory Syndrome Coronavirus (SARS-COV) and Middle East Respiratory Syndrome Coronavirus (MERS-COV) [1].

Initially (01/12/2020) these new coronaviruses were named with 2019-nCOV [2,3] and on 02/11/2020 The International Virus Classification Commission (ICTV) classified the virus as SARS-COV-2 [4]. After the coronavirus was isolated and sequenced, [5] it was discovered that it belongs to the genus β [6,7] of the family Coronaviridae of the order Nidovirales, containing at least four structural proteins: Spike (S), Envelope (E), Membrane (M) and Nucleocapsid (N) [4]. Since then, in the fight against the coronavirus, scientists have used several strategies to develop new drugs [8].

For the development of drugs for the treatment of SARS-COV-2, the quickest way is to find potential molecules available on the drug market (Drug Repurposing). Drug repurposing can be achieved by conducting systematic drug-drug target interaction and drug-drug interaction analyzes [9]. A survey on drug-drug target interaction collected by the DrugBank database [10] found that on average each drug has 3 drug targets and each drug target has 4.7 drugs [11].

Scientists worldwide have proposed the use of preexisting drugs against the novel coronavirus [12]. Others reported repurposing the use of existing antiviral agents in order to reduce time and cost compared to the new drug discovery [13]. Studies related to the reuse of drugs for the treatment of COVID-19 has been looking for inhibitors of SARS-COV-2 main protease (M^{pro}) that are essential for viral replication and transcription [14-29] and of SARS-COV-2 Spike Protein [4[30], a glycoprotein that gives coronaviruses a crown-like appearance like by forming spikes on their surface [1]. The SARS-COV-2 Spike protein binds to ACE-2 receptor proteins (angiotensin converting enzyme 2) on cell surfaces to infect the host [1,4], [31-34].

Within this context, Micholas D. Smith and Jeremy C. Smith both from the University of Tennessee used the world's most powerful computer, SUMMIT, to carry out a high-throughput virtual screening campaign and identify molecules to bind to isolated protein S or even on the $S_{protein}$-$ACE2_{human}$ interface [30]. In this work, the authors performed 100,000 docking calculations that generated 8669 scores of conformations of molecules linked to the $S_{protein}$-

* Corresponding author. ORCID: https://orcid.org/0000-0001-6094-3826.
E-mail address: sehenriquefaria@usp.br (S.H.D.M. Faria).

https://doi.org/10.1016/j.molstruc.2021.130076
0022-2860/

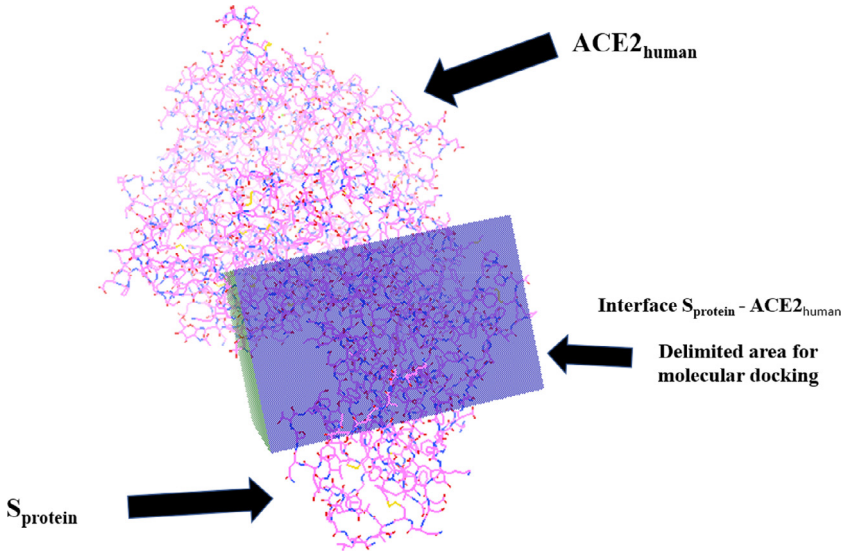

Fig. 1. Delimitation of the molecular docking area on the $S_{protein}$-$ACE2_{human}$ interface in the Autodock 4.2.6 program, whose box generated 605085 Grid Points per Map.

$ACE2_{human}$ interface, with the molecules with the highest scores (nitrofurantoin, isozianide pyruvate and eriodictyol).

Although the docking technique performs a virtual screening through scores, it cannot describe the electronic behavior of drugs coupled to the $S_{protein}$-$ACE2_{human}$ interface. Two techniques capable of accurately describing electronic density are the theories QTAIM [35] and IQA [36]. They have already been used by our research group to describe the mechanism of action of the drugs Mechlorethamine [37], 5-Fluoracil [38] and Carmustine [39]. The location and characterization of critical points related to hydrogen bonds were essential for determining the chemical mechanism of these three drugs.

Another interaction that proves to be important for drug-site stabilization is H-H closed-shell interactions [40]. The first report of this interaction took place in a low temperature neutron diffraction crystallography experiment in 1983 [41]. Subsequently, in 1985, Reid [42] reported this same interaction from crossed molecular beam experiments. Weak dihydrogen bonds between hydrogen of the methyl group and a hydrogen of an amine group were found in four rotamers of the amino acid leucine by Matta and Bader [43]. Thus, there is rich evidence that suggests that this H-H interaction stabilizes systems in which it is a part [44], with its existence and importance in byphenyl reviewed by Trujillo and Matta [45].

Thus, the objective of this paper is to use the theories QTAIM and IQA to locate and quantify sites of interaction between the five drugs most punctuated by the Docking technique performed on the $S_{protein}$-$ACE2_{human}$ interface obtained on the SUMMIT computer by researchers at the University of Tennessee.

2. Calculations

To perform the molecular coupling, we prepared the same $S_{protein}$-$ACE2_{human}$ interface model used in the work of researchers at the University of Tennessee, with the aim of simulating environments similar to that used in their dockings [30]. For this, we used a $S_{protein}$-ACE_{human} obtained by Li and collaborators [46] deposited in the PDB DATA BANK [47] with the ID: 2AJF.

Using the Autodock 4.2.6 [48] software with the aid of AutoDockTools (version mgltools.1.5.6) we made the molecular docking of the five most scored inhibitors in Smith's work [30] (ligands 3223, 3362, 1629, 2542 and 2600 - in decreasing order of score).

After removing the water from the crystal, a box was built on the $S_{protein}$-$ACE2_{human}$ interface to determine and limit the docking region. The coordinates (x, y and z) of the box had maximum values of 11.539, 13.912 and 78.261 and minimum of -16.077, -26.548 and 42.297. The Autodock used 605085 Grid Points per Map (grid points inside the box) and made a smooth of 0.5. The positioning of the box was placed at the bottom of the $ACE2_{human}$ protein and covered up to half the structure of $S_{protein}$ (Figure 1). To perform molecular docking, Autodock used the Lamarckian genetic algorithm.

The Autodock generated 50 conformations of the ligands positioned on the $S_{protein}$-$ACE2_{human}$ interface, where the 30 most scored geometries were visualized in the Chimera 1.14 [49] program, which enabled the identification of the amino acid residues of the two proteins that interact with the ligands (Figure 2).

In this way, a screening was carried out and only the geometric conformations of the ligands that contained interactions between the amino acids of the $S_{protein}$ and/or $ACE2_{human}$ proteins were separated. Once these conformations were identified, they were manipulated in the GaussView5.0 [50] program where all the amino acid residues that did not interact with the ligand were erased. Thus, the resulting molecular clusters were subjected to a single point calculation in the Gaussian09 [51] software to generate the file that describes the wave function of each conformation, the .wfn file. All of these single point calculations were performed at the B3LYP/6-31G level (d, p).

After this step, the .wfn files were submitted to the AIMALL [52] computational package to perform the electronic density, Laplacian electronic density and charge (QTAIM) calculations in addition to the energy decomposition values of the IQA method. All of these calculations were performed using the default parameters of the AIMALL software.

3. Results and Discussion

3.1. Molecular Docking between the $S_{protein}$-$ACE2_{human}$ interface and possible inhibitors of SARS-COV-2 infection

The most scored ligands in the molecular docking of reference 31 were molecules number 3223, 3362, 1629, 2542 and 2600. The official IUPAC name for each molecule is highlighted in Table 1.

The molecular docking performed by Autodock 4.2.6 between the $S_{protein}$-$ACE2_{human}$ interface and the molecules of Table 1 gen-

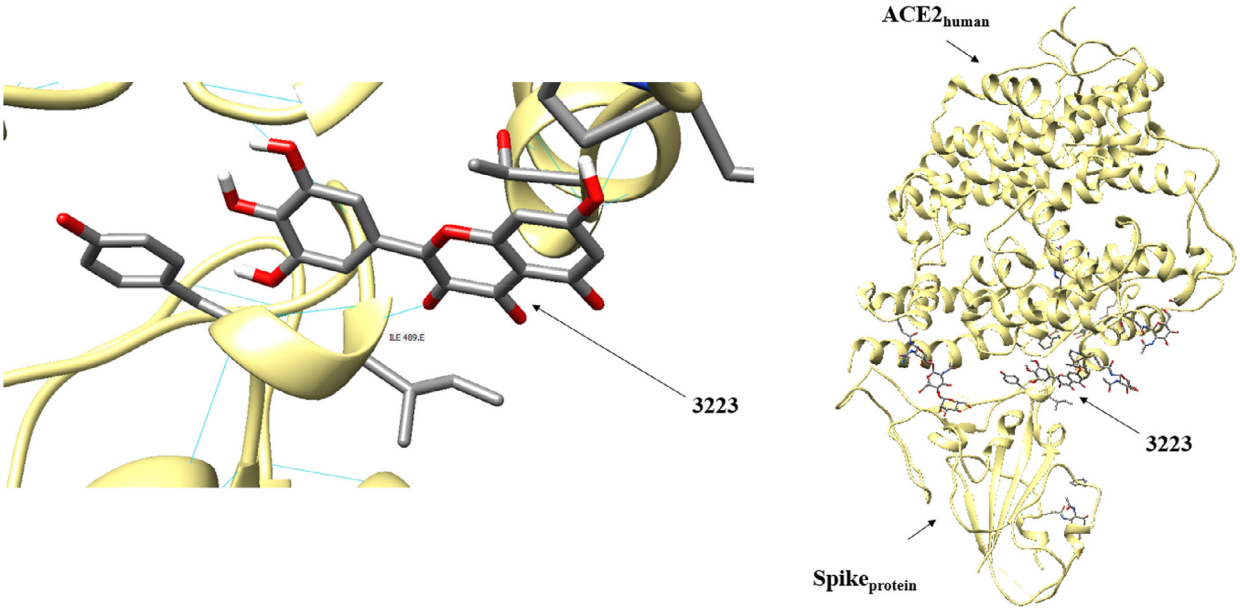

Fig. 2. Positioning of the 3223 molecule at the $S_{protein}$-$ACE2_{human}$ interface performed by the docking method.

Table 1
IUPAC official name of the ligands used in molecular docking in the $S_{protein}$-$ACE2_{human}$ interface region.

Molecule label	IUPAC Name
3223 (Leucodelphidin)	(2*R*,3*S*,4*S*)-2-(3,4,5-trihydroxyphenyl)-3,4-dihydro-2*H*-chromene-3,4,5,7-tetrol
3362 (Leukoefdin)	2-(3,4,5-trihydroxyphenyl)-3,4-dihydro-2H-1-benzopyran-3,4,5,7-tetrol
1629 (S-8510)	2-(Isoxazol-3-yl)-1,6,7,9-tetrahydroimidazo[4,5-d]pyrano[4,3-b]pyridine
2542	(2s,3r)-2-(3,4-Dihydroxyphenyl)-3,7-dihydroxy-2,3-dihydro-4h-chromen-4-one
2600 (ZINC104875569)	(2S,3S,4S)-2-(4-Hydroxyphenyl)-3,4-dihydro-2H-chromene-3,4,5,7-tetrol

Table 2
Amino acids that promote the interaction between viral Spike and $ACE2_{human}$ proteins on the left side of the table. On the right side, molecules that have hydrogen bonding with (or near) amino acids that promote interactions between $S_{protein}$-$ACE2_{humam}$.

Interface $S_{protein}$-$ACE2_{human}$ interaction site	Molecule	Ranking*	hydrogen interaction location
Tyr (491Spike) - Glu (37ACE2)	3223	16	Ile (489 Spike)
Gly (488Spike) – Lys (353ACE2)	3362	19	Tyr (491 Spike)
Tyr (436Spike) – Gln (42ACE2)	1629	12	Gly (354 ACE2)
Tyr (436Spike) – Asp (38ACE2)	2542	9	Glu (37ACE2)
Tyr (436Sspike) – Asp (38ACE2)	2600	12	Tyr (491 Spike)
Arg (426Spike) – Glu (329ACE2)	2600	23	Tyr (491 Spike)
Thr (486Spike) – Tyr (41ACE2)	2600	26	Glu (37ACE2)

*Ranking is the position of the conformation in the ranking of the molecular coupling of the respective molecule.

erated 50 conformations for each substance. The 30 highest scored conformations were analyzed in the Chimera 1.14 program, which preliminarily tracked the hydrogen bonding interactions between the ligands and the amino acids of the proteins.

Also, intermolecular interactions between Spike protein residues and $ACE2_{human}$ residues were tracked without the presence of any molecules in Table 1. Knowing the binding sites between the two proteins (the amino acid residues that interact with each other forming the $S_{protein}$-$ACE2_{human}$ interface) we eliminated the docking conformations of the molecules that formed hydrogen bonds far from the interaction sites between the viral protein and $ACE2_{human}$.

Table 2 shows the conformations that generated hydrogen bonding close to the binding sites of the $S_{protein}$-$ACE2_{human}$ interface, with their numbering being the ranking position according to their score within the 30 geometries with the highest scores for the molecular docking method.

It is very important to note that almost all molecules are positioned in the region of the interaction site between the amino acids Tyr-491(Spike)-Glu-37(ACE2), with the exception of the 1629 molecule. This shows that this region is the main target in the search for an agent inhibitor of the interaction between tyrosine-491 and glutamic acid-37.

With the structures of the molecules of Table 1 docked in the region between the viral and human proteins, they were used to perform the QTAIM and IQA analyzes.

3.2. QTAIM and IQA analysis between possible infection inhibitors and the amino acids of viral Spike and $ACE2_{human}$ proteins

3.2.1. Interaction between 3223 molecule and isoleucine-489 from the Spike SARS-COV-2 protein

As can be seen from Table 2, the interaction of the 3223 molecule occurs at the amino acid Ile-489($Spike_{protein}$), that is very

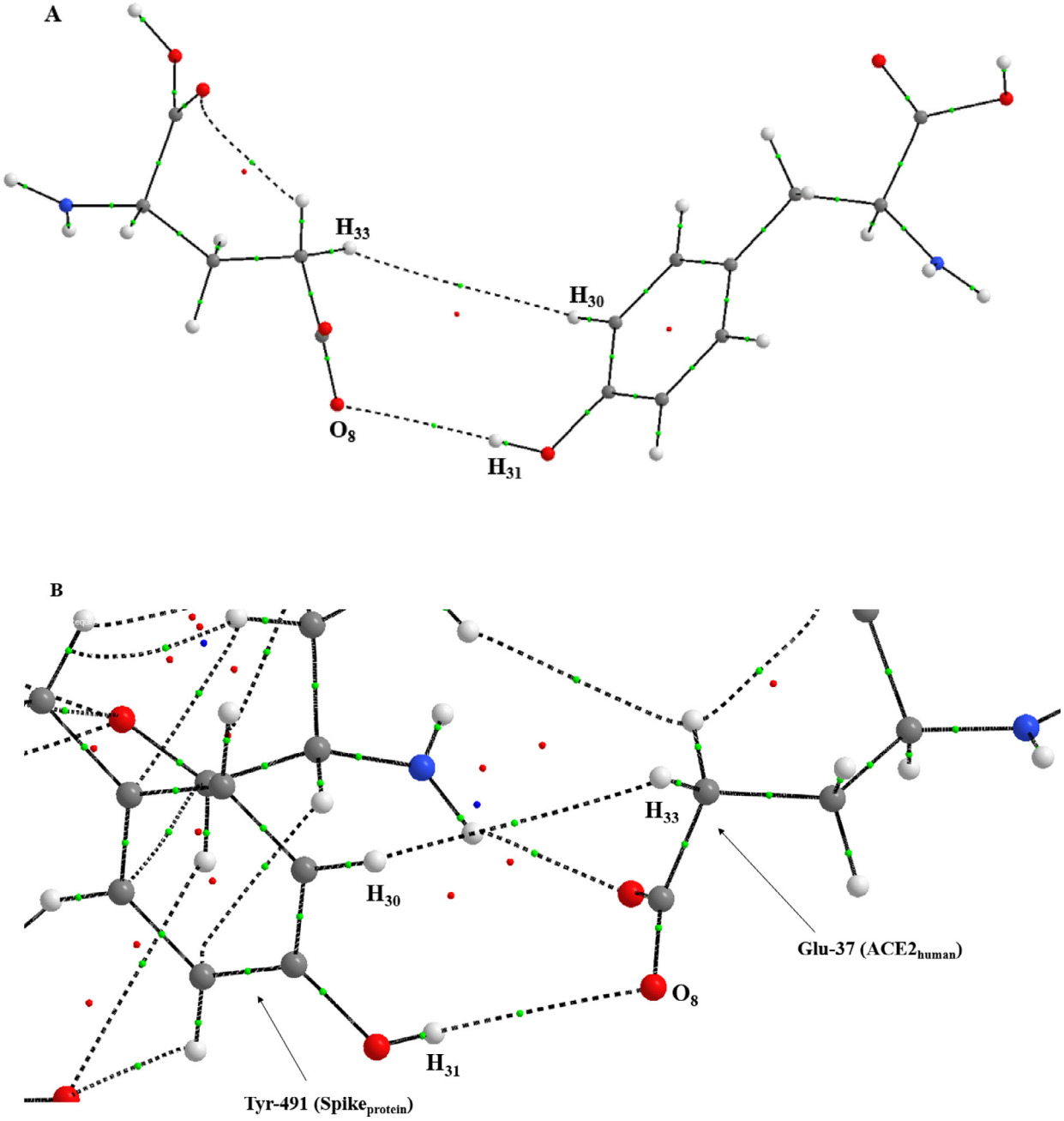

Fig. 3. A) Molecular graph of Tyr-491(Spike)-Glu-37(ACE2) interaction without the presence of the 3223 molecule. B) Molecular graph of Tyr-491(Spike)-Glu-37(ACE2) interaction with the presence of the 3223 molecule.

close to the hydrogen bonding site of the $S_{protein}$-$ACE2_{human}$ interface Tyr-491(Spike)-Glu-37(ACE2) (Figure 2).

Using the electronic density gradient, the critical points were calculated where $\vec{\nabla}\rho(r) = 0$, locating the Nuclear Attractor Critical Points (NAPC), the Bond Critical Points (BCP) and the Ring Critical Points (RCP). With that, we obtained the molecular graph of this molecular cluster in addition to the amino acids Tyr-491(Spike)-Glu-37(ACE2) without the presence of the 3223 molecule (Figure 3). Thus, comparing the values of $\rho(r)$, $\nabla^2\rho(r)$, zero-flux charges (q) and bind energy (E_{bind}) of the interaction site with and without the presence of the cluster 3223-Ile-489 (Table 3), we can determine the interference of the ligand in the interaction between the proteins Spike and $ACE2_{human}$.

The data in Table 3 demonstrate that the presence of the 3223 molecule changed little the electronic density of the atoms that promote the interaction between Tyr-491 and Glu-37. The most significant variance was in the BCP of O_8-H_{31}, which did not mean a decrease in the interaction between the two atoms, since in practice the Laplacian of electronic density varied around 0.4%. The greatest variation of $\nabla^2\rho(r)$ occurred at the critical point of connection H_{30}-H_{33} around 7%, becoming more positive, that is, less covalent and more likely to break, decreasing the interaction between the two hydrogens. There is also a decrease of approximately 1.5% in E_{bind} of H_{31}, decreasing the interaction strength of BCP O_8-H_{31}.

Note that the largest variations are in the zero-flux electrical charge (QTAIM). The presence of the ligand (3223) causes a great polarization of the electronic density of the atoms of the interaction site, mainly between H_{30} and H_{33}, which generates a great variation in charge (~ -421% and 128% respectively). This variation

Table 3
Values of de $\rho(r)$, $\nabla^2\rho(r)$, zero-flux charge (q) and bind energies (IQA) from the Tyr-491(Spike)-Glu-37(ACE2) interaction site before and after the presence of the 3223 molecule nearby. All values are in *a. u.*

Critical Point			With 3223 molecule			Without 3223 molecule		
	$\rho(r)$	$\nabla^2\rho(r)$	E_{bind}	q				
	$\rho(r)$	$\nabla^2\rho(r)$	E_{bind}	q				
H_{31} (Tyr-491)	0.3966	-	-0.3686	0.6120	0.3986	-	-0.3741	0.6036
O_8 (Glu 37)	290.4961	-	-74.6483	-0.8701	290.5631	-	-74.6255	-0.9805
H_{30} (Tyr-491)	0.4353	-	-0.4952	-0.0186	0.4328	-	-0.4928	0.0058
H_{33} (Glu 37)	0.4327	-	-0.4977	0.0164	0.4334	-	-0.4984	0.0072
BCP H_{30}-H_{33}	0.0004	0.0015	-	-	0.0004	0.0014	-	-
BCP O_8-H_{31}	0.0056	0.0223	-	-	0.0055	0.0224	-	-
Critical Point	Δ %							
	$\rho(r)$	$\nabla^2\rho(r)$	E_{bind}	q				
H_{31} (Tyr-491)	-0.5018	-	-1.4702	1.3917				
O_8 (Glu 37)	-0.0231	-	0.0306	-11.2596				
H_{30} (Tyr-491)	0.5776	-	0.4870	-420.6897				
H_{33} (Glu 37)	-0.1615	-	-0.1404	127.7778				
BCP H_{30}-H_{33}	0.0000	7.1429	-	-				
BCP O_8-H_{31}	1.8182	-0.4464	-	-				

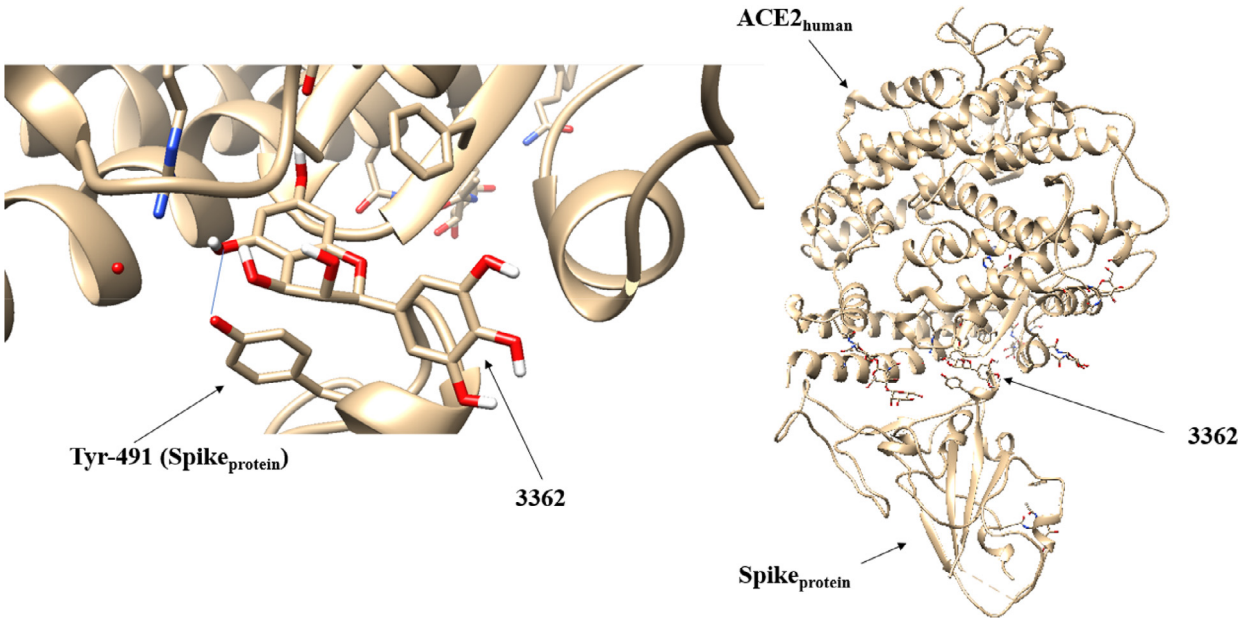

Fig. 4. Positioning of the 3362 molecule at the $S_{protein}$-$ACE2_{human}$ interface performed by the docking method.

in the charge of hydrogens explains the variation of $\nabla^2\rho(r)$ of the BCP H_{30}-H_{33}, which decreases the interaction between $Spike_{protein}$-$ACE2_{human}$ proteins.

3.2.2. Interaction of 3362 molecule and tyrosine-491 from the Spike SARS-COV-2 protein

The positioning of the 3362 molecule at the $S_{protein}$-$ACE2_{human}$ interface was performed by molecular docking that generated a hydrogen interaction between the ligand and the amino acid tyrosine 491 of the viral Spike protein, as can be seen in Figure 4.

The gradient of electronic density allowed us to find the critical points of cluster 3362-Tyr-491(Spike)-Glu-37(ACE2) and build its molecular graph (Figure S1). The QTAIM and IQA parameters of these critical points are shown in Table 4. It can be noted that the presence of this ligand generated little variation in the calculated parameters, except for the QTAIM charge of the H_{30} and H_{33} hydrogens.

This caused the greatest variations in E_{bind} (IQA) in exactly these two atoms, indicating that this interaction between the two proteins (Spike and ACE2) is the most fragile. Despite variations in E_{bind} of around 1%, the molecule 3362 will probably not break or significantly decrease the interaction between the amino acids Tyr-491(Spike) and Glu-37(ACE2).

3.2.3. Interaction of 1629 molecule and glycine-354 from the Spike SARS-COV-2 protein

In the case of the 1629 molecule, the molecular docking technique positioned it close to the interaction site Gly-488(Spike) - Lys-353(ACE2) in which it generated a hydrogen interaction in the amino acid glycine-354(ACE2) - Figure 5. Similar to the previous molecules, the gradient of the electronic density located the critical points generating the molecular graph of this system (Figure S2).

Through the data in Table 5, again the atomic electrical charges showed the greatest variation, being approximately 8.5% greater in the presence of ligand 1629 for the O_4 atom. Probably this increase in charge on the oxygen atom originated in the displacement of the electronic density of the ligand to the critical point of attachment O_4-N_{10}, which presented an increase of ~ 2.7% in its $\rho(r)$. This resulted in a negative variation of ~ 3.4% in BCP O_4-N_{10}, decreasing the interaction between the two proteins, Spike and ACE2. Despite that, the decrease in E_{bind} was at most 0.03% for O_4. Anyway, the

Table 4
Values of de $\rho(r)$, $\nabla^2\rho(r)$, zero-flux charge (q) and bind energies (IQA) from the Tyr-491(Spike)-Glu-37(ACE2) interaction site before and after the presence of the 3362 molecule nearby. All values are in *a. u.*

Critical Point			With 3362 molecule			Without 3362 molecule		
	$\rho(r)$	$\nabla^2\rho(r)$	E_{bind}	q				
	$\rho(r)$	$\nabla^2\rho(r)$	E_{bind}	q				
H_{31} (Tyr-491)	0.3975	-	-0.3762	0.6061	0.3986	-	-0.3741	0.6036
O_8 (Glu 37)	290.5748	-	-74.609	-1.0210	290.5631	-	-74.6255	-0.9805
H_{30} (Tyr-491)	0.4337	-	-0.4978	0.0043	0.4328	-	-0.4928	0.0058
H_{33} (Glu 37)	0.4333	-	-0.4931	0.0034	0.4334	-	-0.4984	0.0072
BCP H_{30}-H_{33}	0.0004	0.0014	-	-	0.0004	0.0014	-	-
BCP O_8-H_{31}	0.0054	0.0223	-	-	0.0055	0.0224	-	-
Critical Point	Δ %							
	$\rho(r)$	$\nabla^2\rho(r)$	E_{bind}	q				
H_{31} (Tyr-491)	-0.2760	-	0.5613	0.4142				
O_8 (Glu 37)	0.0040	-	-0.0221	4.1305				
H_{30} (Tyr-491)	0.2079	-	1.0146	-25.8621				
H_{33} (Glu 37)	-0.0231	-	-1.0634	-52.7778				
BCP H_{30}-H_{33}	0.0000	0.0000						
BCP O_8-H_{31}	-1.8182	-0.4464						

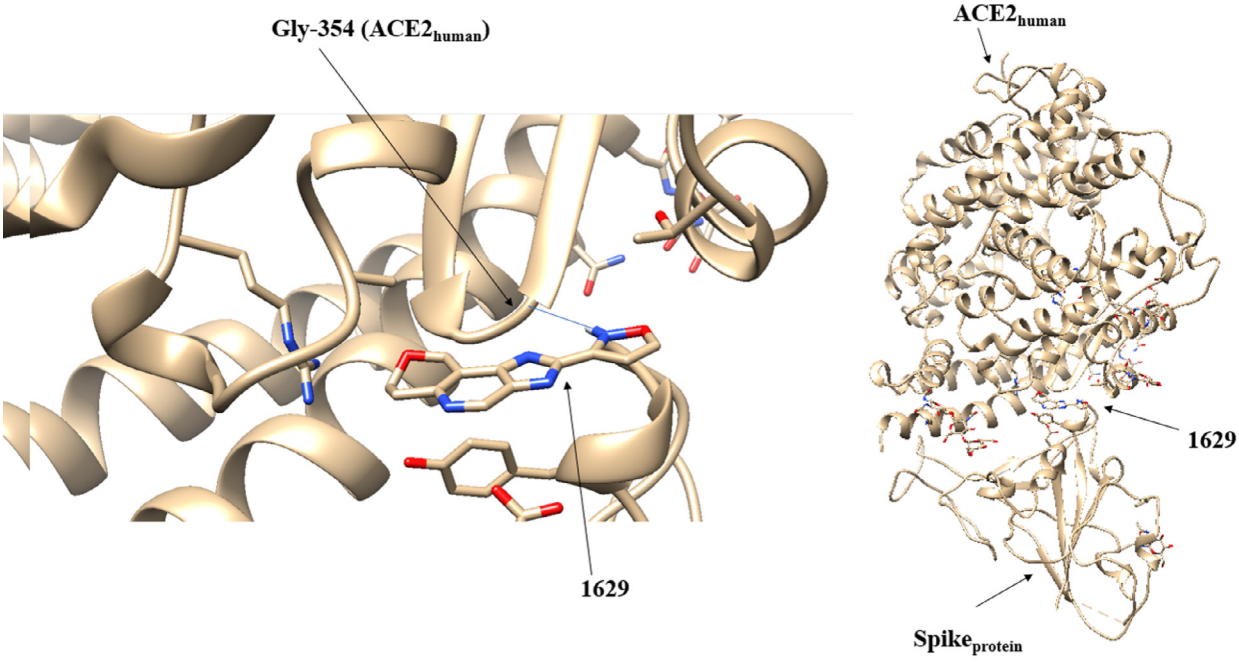

Fig. 5. Positioning of the 1629 molecule at the $S_{protein}$-$ACE2_{human}$ interface performed by the molecular docking method.

Table 5
Values of de $\rho(r)$, $\nabla^2\rho(r)$, zero-flux charge (q) and bind energies (IQA) from Gly-488(Spike)-Lys-353(ACE2) interaction site before and after the presence of the 1629 molecule nearby. All values are in *a. u.*

Critical Point			With 1629 molecule			Without 1629 molecule		
	$\rho(r)$	$\nabla^2\rho(r)$	E_{bind}	q	$\rho(r)$	$\nabla^2\rho(r)$	E_{bind}	q
N_{10}	190.2553	-	-54.2292	-1.1048	190.2424	-	-54.2275	-1.1027
O_4	290.4189	-	-74.5915	-1.1971	290.5271	-	-74.6131	-1.1031
O_4-N_{10}	0.0219	0.0854	-	-	0.0225	0.0884	-	-
Critical Point	Δ %							
	$\rho(r)$	$\nabla^2\rho(r)$	E_{bind}	q				
N_{10}	0.0068	-	0.0031	0.1904				
O_4	-0.0372	-	-0.0289	8.5214				
O_4-N_{10}	-2.6667	-3.3937	-	-				

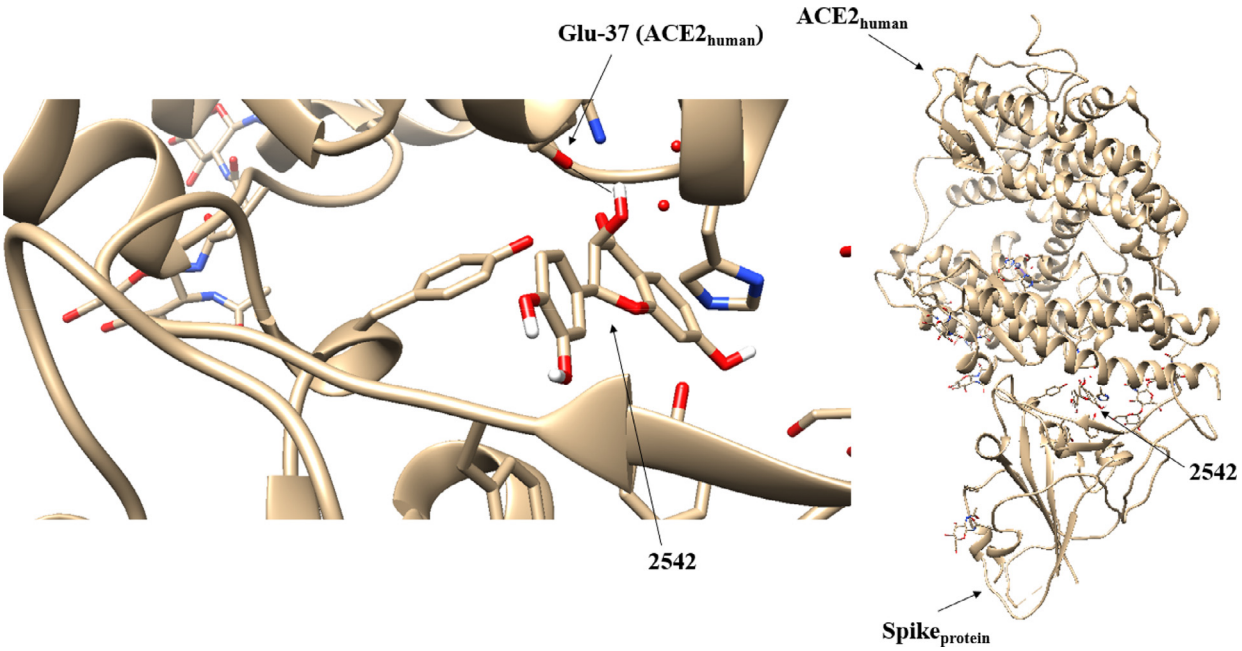

Fig. 6. Positioning of the 2542 molecule at the $S_{protein}$-$ACE2_{human}$ interface performed by the molecular docking method.

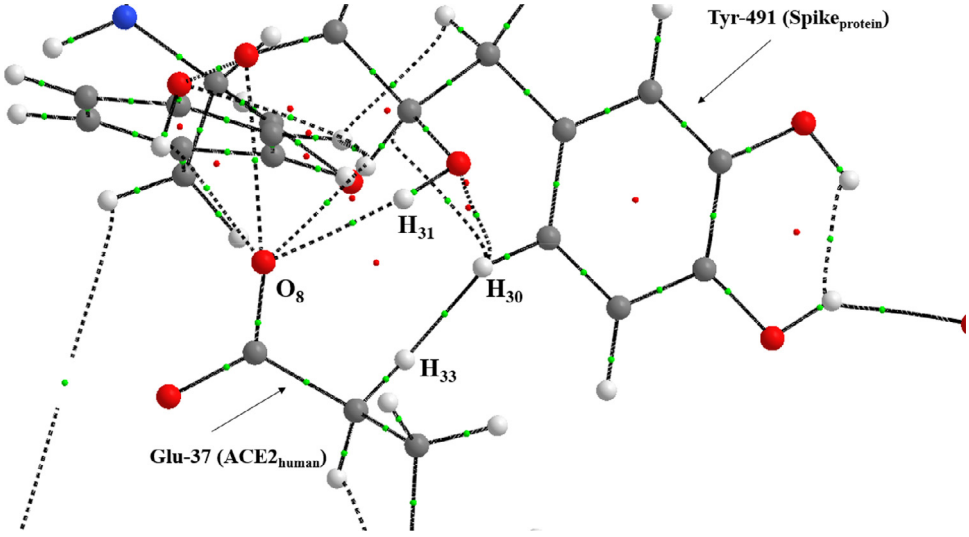

Fig. 7. Molecular graph of the Tyr-491(Spike)-Glu-37(ACE2) interaction with the presence of the 2542 molecule.

data from the 1629 molecule make it a great candidate to be tested *in vitro* tests.

3.2.4. Interaction of 2542 molecule and glutamic acid-37 from the Spike SARS-COV-2 protein

The use of the molecular docking technique applied to the 2542 molecule positioned it at the Tyr-491(Spike)-Glu-37(ACE2) site, however, this time, the ligand interacts with the amino acid Glu-37 instead of Tyr-491 (Figure 6).

The molecular graph (Figure 7) that located all the critical points of this system shows the intense interference of the 2542 molecule in the O_8 of Glu-37. The data of the QTAIM and IQA parameters (Table 6) demonstrate a great variation in the electrical charge of the atoms of the two regions of interaction of this binding site. In particular, the H_{30} and H_{33} hydrogens showed a huge change in their electrical charges (~ 266% and ~ 72% respectively). This generated a sudden electronic polarization of these atoms that intensely changed the electronic distribution of the BCP H_{30}-H_{33}. These data indicate that ligand 2542 interfered significantly blocking the interaction between $Spike_{protein}$-$ACE2_{human}$ in that region.

It is interesting to note that O_8, which is one of the atoms promoting the attraction interaction between viral and human proteins, also undergoes great variation in its electrical charge (~18%). This variation in its electrical charge affects the electronic density, increasing its polarization, which generated a sudden change in its Laplacian. The increase in the positive value of $\nabla^2\rho(r)$ tends to increase the ionic character of BCP O_8-H_{31}, decreasing its covalence and consequently its ability to interact.

As ligand 2542 presented interaction reduction action in the two regions of interaction of the Tyr-491(Spike)-Glu-37(ACE2) site: BCPs O_8-H_{31} and H_{30}-H_{33}, this molecule proves to be the best candidate for tests inhibition of the SARS-COV-2 virus.

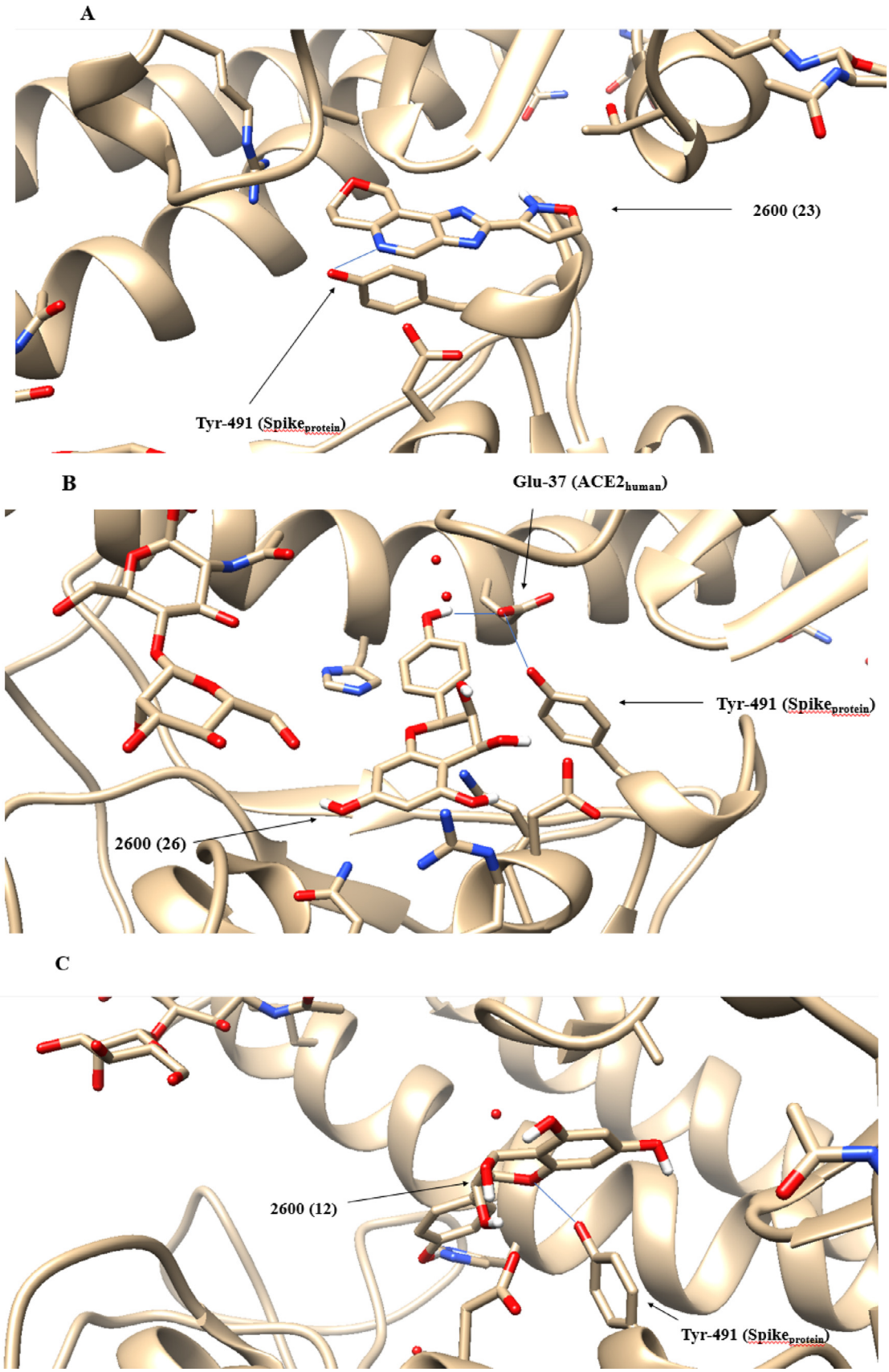

Fig. 8. Positioning of the 2600 molecule at the $S_{protein}$-$ACE2_{human}$ interface: A) Positioning of conformation 23. B) Positioning of conformation 26. C) Positioning of conformation 12.

Table 6
Values of de $\rho(r)$, $\nabla^2\rho(r)$, zero-flux charge (q) and bind energies (IQA) from the Tyr-491(Spike)-Glu-37(ACE2) interaction site before and after the presence of the 2542 molecule nearby. All values are in *a. u.*

Critical Point			With 2542 molecule			Without 2542 molecule		
	$\rho(r)$	$\nabla^2\rho(r)$	E_{bind}	q	$\rho(r)$	$\nabla^2\rho(r)$	E_{bind}	q
H_{31} (Tyr-491)	0.3906	-	-0.3694	0.6279	0.3986	-	-0.3741	0.6036
O_8 (Glu 37)	290.4034	-	-74.5934	-1.1542	290.5631	-	-74.6255	-0.9805
H_{30} (Tyr-491)	0.4362	-	-0.4887	-0.0096	0.4328	-	-0.4928	0.0058
H_{33} (Glu 37)	0.4439	-	-0.4967	0.0020	0.4334	-	-0.4984	0.0072
BCP H_{30}-H_{33}	0.0061	0.0232	-	-	0.0004	0.0014	-	-
BCP O_8-H_{31}	0.0056	0.0242	-	-	0.0055	0.0224	-	-
Critical Point	Δ %							
	$\rho(r)$	$\nabla^2\rho(r)$	E_{bind}	q				
H_{31} (Tyr-491)	-2.0070	-	-1.2563	4,0258				
O_8 (Glu 37)	-0.0550	-	-0.0430	17,7155				
H_{30} (Tyr-491)	0.7856	-	-0.8320	-265,5172				
H_{33} (Glu 37)	2.4227	-	-0.3411	-72,2222				
BCP H_{30}-H_{33}	1425.0000	1557.1429	-	-				
BCP O_8-H_{31}	1.8182	8.0357	-	-				

Table 7
Values of $\rho(r)$, $\nabla^2\rho(r)$, zero-flux charge (q) and E_{bind} (IQA) of the Tyr-491(Spike)-Glu -37(ACE2) interaction site before and after the presence of the 2600 molecule in conformations 12, 23 and 26. All values are in *a. u.*

Critical Point			With 2600 (12) molecule			Without 2600 (12) molecule		
	$\rho(r)$	$\nabla^2\rho(r)$	E_{bind}	q	$\rho(r)$	$\nabla^2\rho(r)$	E_{bind}	q
H_{31} (Tyr-491)	0.3970	-	-0.3730	0.6053	0.3986	-	-0.3741	0.6036
O_8 (Glu 37)	290.4595	-	-74.5811	-1.0895	290.5631	-	-74.6255	-0.9805
H_{30} (Tyr-491)	0.4328	-	-0.4978	0.0150	0.4328	-	-0.4928	0.0058
H_{33} (Glu 37)	0.4364	-	-0.4950	-0.0194	0.4334	-	-0.4984	0.0072
BCP H_{30}-H_{33}	0.0004	0.0015	-	-	0.0004	0.0014	-	-
BCP O_8-H_{31}	0.0058	0.0224	-	-	0.0055	0.0224	-	-
Critical Point	With 2600 (23) molecule	Without 2600 (23) molecule						
	$\rho(r)$	$\nabla^2\rho(r)$	E_{bind}	q	$\rho(r)$	$\nabla^2\rho(r)$	E_{bind}	q
H_{31} (Tyr-491)	0.4087	-	-0.3740	0.5723	0.3986	-	-0.3741	0.6036
O_8 (Glu 37)	290.5349	-	-74.6260	-1.0172	290.5631	-	-74.6255	-0.9805
H_{30} (Tyr-491)	0.4331	-	-0.4981	0.0106	0.4328	-	-0.4928	0.0058
H_{33} (Glu 37)	0.4332	-	-0.4931	0.0023	0.4334	-	-0.4984	0.0072
BCP H_{30}-H_{33}	0.0004	0.0015	-	-	0.0004	0.0014	-	-
BCP O_8-H_{31}	0.0058	0.0228	-	-	0.0055	0.0224	-	-
Critical Point	With 2600 (26) molecule	With 2600 (26) molecule						
	$\rho(r)$	$\nabla^2\rho(r)$	E_{bind}	q	$\rho(r)$	$\nabla^2\rho(r)$	E_{bind}	q
H_{31} (Tyr-491)	0.3914	-	-0.3655	0.6255	0.3986	-	-0.3741	0.6036
O_8 (Glu 37)	290.2761	-	-74.6035	-1.2042	290.5631	-	-74.6255	-0.9805
H_{30} (Tyr-491)	0.4345	-	-0.4925	-0.0291	0.4328	-	-0.4928	0.0058
H_{33} (Glu 37)	0.4368	-	-0.4952	-0.0257	0.4334	-	-0.4984	0.0072
BCP H_{30}-H_{33}	0.0002	0.0012	-	-	0.0004	0.0014	-	-
BCP O_8-H_{31}	0.0058	0.0233	-	-	0.0055	0.0224	-	-
Critical Point	Δ% (2600-12)	Δ% (2600-23)						
	$\rho(r)$	$\nabla^2\rho(r)$	E_{bind}	q	$\rho(r)$	$\nabla^2\rho(r)$	E_{bind}	q
H_{31} (Tyr-491)	-0.4014	-	31.3018	0.2816	2.5339	-	-0.0267	-5.1856
O_8 (Glu 37)	-0.0357	-	-0.0595	11.1168	-0.0097	-	0.0007	3.7430
H_{30} (Tyr-491)	0.0000	-	0.4464	158.6207	0.0693	-	1.0755	82.7586
H_{33} (Glu 37)	0.6922	-	-0.1204	-369.4444	-0.0461	-	-1.0634	-68.0556
BCP H_{30}-H_{33}	0.0000	7.1429	-	-	0.0000	7.1429	-	-
BCP O_8-H_{31}	5.4545	0.0000	-	-	5.4545	1.7857	-	-
Critical Point	Δ% (2600-26)							
	$\rho(r)$	$\nabla^2\rho(r)$	E_{bind}	q				
H_{31} (Tyr-491)	-1.8063	-	-2.2989	3.6282				
O_8 (Glu 37)	-0.0988	-	-0.0295	22.8149				
H_{30} (Tyr-491)	0.3928	-	-0.0609	-601.7241				
H_{33} (Glu 37)	0.7845	-	-0.6421	-456.9444				
BCP H_{30}-H_{33}	-50.0000	-14.2857	-	-				
BCP O_8-H_{31}	5.4545	4.0179	-	-				

3.2.5. Interaction of 2600 molecule and tyrosine-491 from the Spike SARS-COV-2 protein and glutamic acid-37 from ACE2$_{human}$ protein

The molecular docking technique generated three conformations of the 2600 molecule that promoted hydrogen interactions in amino acids of the $S_{protein}$-$ACE2_{human}$ interface. These conformations were 12, 23 and 26 and their interactions occurred in residues Tyr-491(Spike), Tyr-491(Spike) and Glu-37(ACE2) respectively. However, the three conformations occurred at the same interaction site. The positioning of each conformation of the molecule at the $S_{protein}$-$ACE2_{human}$ interface can be seen in Figure 8.

The molecular graphs generated by the location of the critical points of these 3 systems are available in Figure S3. The data for the QTAIM and E_{bind} (IQA) parameters in Table 7 show that in the

three conformations of the 2600 molecule, there was a great variation in the electric charge in the H_{30} and H_{31} hydrogens, with great emphasis on the conformation 26.

While conformations 12 and 23 showed identical changes in the Laplacian of the electronic density of BCP H_{30}-H_{31}, conformation 26 presented almost twice the percentage variation of this quantity at this critical point, due to the great loss of $\rho(r)$ in the region between the H_{30} and H_{31} (-50.000 au). This value suggests a significant drop in the interaction between Spike and $ACE2_{human}$ proteins.

This suggestion is corroborated by the significant drop of $\nabla^2\rho(r)$ (-14.2857 a.u.) which demonstrates a drop in the covalence of the chemical bond making the 2600 molecule a candidate for laboratory tests.

4. Conclusions

The structures of the proteins Spike and $ACE2_{human}$ obtained in the PDB DATA BANK showed seven sites of interaction between them. However, the molecular docking technique positioned four ligands at the Tyr-491(Spike)-Glu-37(ACE2) site and one ligand at the Gly-488 (Spike)-Lys-353(ACE2) site.

The data QTAIM and IQA (E_{bind}) demonstrated that molecules 3223 and 3362 do not have capacities that allow them to cause an inhibitory effect on the attraction between viral and human proteins. The 1629 molecule, on the other hand, had the potential to decrease the interaction between the protein Spike and ACE2 at the interaction site Gly-488(Spike)-Lys-353(ACE2) because it decreases by approximately 3.4% the value of $\nabla^2\rho(r)$ in BCP O_4-N_{10}.

The 2542 and 2600 molecules showed significant interactions that decrease the attractive effect of the Spike protein on the Tyr-491(Spike)-Glu-37(ACE2) site, with emphasis on the 2542 ligand that decreases the attraction in the two BCPs of this interaction site. Thus, our results suggest laboratory tests combining the effect of the 1629 molecule with those of the 2542 and 2600 molecules, as this way the inhibitory effect could occur at two binding sites simultaneously, with greater expectation in the 1629/2542 combination.

The data also demonstrated that the presence of all ligands created large changes in electrical charges in the atoms responsible for the interactions between the proteins Spike and ACE2. Thus, the use of non-neutral binders (electrically charged) can present significant inhibitory results, opening the possibility of studies for laboratory tests and also theoretical ones that apply hybrid MM/QM methods.

Author Contributions

Sergio H. D. M. Faria – Manipulation of docking data in the Chimera 1.14 software, performing QTAIM and IQA calculations in the AIMALL program, creating figures and tables, interpreting data and preparing the manuscript.

João G. Teleschi – Performing molecular docking calculations using Autodock 4.2.6 software.

Competing Financial of Interest

The authors declare no competing financial interest.

Declaration of Competing Interest

The authors declare that they have no known competing financial interests or personal relationships that could have appeared to influence the work reported in this paper.

The authors declare the following financial interests/personal relationships which may be considered as potential competing interests.

Acknowledgment

We would like to thank Professor Roy Edward Bruns of the Unicamp Chemistry's Institute by lending us his computational center for performing the calculations with AIMAll.

Supplementary materials

Supplementary material associated with this article can be found, in the online version, at doi:10.1016/j.molstruc.2021.130076.

References

[1] Y. Chen, Y. Guo, Y. Pan, Z. Zhao, Structure analysis of the receptor binding of 2019-nCoV, Biochem. Biophys. Res. Commun. 525 (2020) 135.
[2] N. Zhu, D. Zhang, W. Wang, X. Li, B. Yang, J. Song, X. Zhao, B. Huang, W. Shi, R. Lu, P. Niu, F. Zhan, X. Ma, D. Wang, W. Xu, G. Wu, G. Gao, W. Tan, A Novel Coronavirus from Patients with Pneumonia in China, N. Engl. J. Med. 382 (2020) (2019) 727.
[3] Y. Chen, Q. Liu, D. Guo, Emerging coronaviruses: Genome structure, replication, and pathogenesis, J. Med. Virol. 92 (2020) 2249.
[4] C. Wu, Y. Liu, Y. Yang, P. Zhang, W. Zhong, Y. Wang, Q. Wang, Y. Xu, M. Li, X. Li, M. Zheng, L. Chen, H. Li, Analysis of therapeutic targets for SARS-CoV-2 and discovery of potential drugs by computational methods, Acta Pharm. Sin. B. 10 (2020) 766.
[5] P. Zhou, X. Yang, X. Wang, B. Hu, L. Zhang, W. Zhang, H. Si, Y. Zhu, B. Li, C. Huang, H. Chen, J. Chen, Y. Luo, H. Guo, R. Jiang, M. Liu, Y. Chen, X. Shen, X. Wang, X. Zheng, K. Zhao, Q. Chen, F. Deng, L. Liu, B. Yan, F. Zhan, Y. Wang, G. Xiao, Z. Shi, A pneumonia outbreak associated with a new coronavirus of probable bat origin, Nature 579 (2020) 270.
[6] J. Chan, K. Kok, Z. Zhu, H. Chu, K. To, S. Yuan, K. Yuen, Genomic characterization of the 2019 novel human-pathogenic coronavirus isolated from a patient with atypical pneumonia after visiting Wuhan, Emerg. Microbes & Infect. 9 (2020) 221.
[7] R. Lu, X. Zhao, J. Li, P. Niu, B. Yang, H. Wu, W. Wang, H. Song, B. Huang, N. Zhu, Y. Bi, X. Ma, F. Zhan, L. Wang, T. Hu, H. Zhou, Z. Hu, W. Zhou, L. Zhao, J. Chen, Y. Meng, J. Wang, Y. Lin, J. Yuan, Z. Xie, J. Ma, W. Liu, D. Wang, W. Xu, E. Holmes, G. Gao, G. Wu, W. Chen, W. Shi, W. Tan, Genomic characterisation and epidemiology of 2019 novel coronavirus: implications for virus origins and receptor binding, Lancet 395 (2020) 565.
[8] M. Rahman, T. Saha, K. Islam, R. Suman, S. Biswas, E. Rahat, M. Hossen, R. Islam, M. Hossain, A. Al Mamun, M. Khan, M. Ali, M. Halim, Virtual screening, molecular dynamics and structure-activity relationship studies to identify potent approved drugs for Covid-19 treatment, J. Biomol. Struct. Dyn. (2020), doi:10.1080/07391102.2020.1794974.
[9] J. Wang, Fast Identification of Possible Drug Treatment of Coronavirus Disease-19 (COVID-19) through Computational Drug Repurposing Study, J. Chem. Inf. Model. 60 (2020) 3277.
[10] V. Law, C. Knox, Y. Djoumbou, T. Jewison, A. Guo, Y. Liu, A. Maciejewski, D. Arndt, M. Wilson, V. Neveu, A. Tang, G. Gabriel, C. Ly, S. Adamjee, Z. Dame, B. Han, Y. Zhou, D. Wishart, DrugBank 4.0: shedding new light on drug metabolism, Nucleic Acids Res 42 (2014) D1091.
[11] J. Wang, Y. Ge, X. Xie, Development and Testing of Druglike Screening Libraries, J. Chem. Inf. Model. 59 (2019) 53.
[12] S. Aftab, M. Ghouri, M. Masood, Z. Haider, Z. Khan, A. Ahmad, N. Munawar, Analysis of SARS-CoV-2 RNA-dependent RNA polymerase as a potential therapeutic drug target using a computational approach, J. Transl. Med. 18 (2020) 275.
[13] H. Jia, P. Gong, A Structure-Function Diversity Survey of the RNA-Dependent RNA Polymerases From the Positive-Strand RNA Viruses, Front. Microbiol. 10 (2019) 1945.
[14] A. Andrianov, Y. Kornoushenko, A. Karpenko, I. Bosko, A. Tuzikov, Computational discovery of small drug-like compounds as potential inhibitors of SARS-CoV-2 main protease, J. Biomol. Struct. Dyn. (2020) 10.180/07391102.2020.1792989.
[15] A. Adeoye, B. Oso, I. Olaoye, H. Tijjani, A. Adebayo, Repurposing of chloroquine and some clinically approved antiviral drugs as effective therapeutics to prevent cellular entry and replication of coronavirus, J. Biomol. Struct. Dyn. (2020) 10.180/07391102.2020.1765876.
[16] M. Babadaei, A. Hasan, Y. Vahdani, S. Bloukh, M. Sharifi, E. Kachooei, S. Haghighat, M. Falahati, Development of remdesivir repositioning as a nucleotide analog against COVID-19 RNA dependent RNA polymerase, J. Biomol. Struct. Dyn. (2020) 10.180/07391102.2020.1767210.
[17] S. Enmozhi, K. Raja, I. Sebastine, J. Joseph, Andrographolide as a potential inhibitor of SARS-CoV-2 main protease: an in silico approach, J. Biomol. Struct. Dyn. (2020) 10.180/07391102.2020.1760136.
[18] M. Hendaus, Remdesivir in the treatment of coronavirus disease 2019 (COVID-19): a simplified summary, J. Biomol. Struct. Dyn. (2020) 10.180/07391102.2020.1767691.
[19] R. Khan, R. Jha, G. Amera, M. Jain, E. Singh, A. Pathak, R. Singh, J. Muthukumaran, A. Singh, Targeting SARS-CoV-2: a systematic drug repurposing approach to identify promising inhibitors against 3C-like pro-

teinase and 2 '-O-ribose methyltransferase, J. Biomol. Struct. Dyn. (2020) 10.180/07391102.2020.1753577.
[20] S. Khan, K. Zia, S. Ashraf, R. Uddin, Z. Ul-Haq, Identification of chymotrypsin–like protease inhibitors of SARS-CoV-2 via integrated computational approach, J. Biomol. Struct. Dyn. (2020) 10.180/07391102.2020.1751298.
[21] X. Liu, X. Wang, Potential inhibitors against 2019-nCoV coronavirus M protease from clinically approved medicines, J. Genet. Genomics. 47 (2020) 119.
[22] N. Muralidharan, R. Sakthivel, D. Velmurugan, M. Gromiha, Computational studies of drug repurposing and synergism of lopinavir, oseltamivir and ritonavir binding with SARS-CoV-2 protease against COVID-19, J. Biomol. Struct. Dyn. (2020) 10.180/07391102.2020.1752802.
[23] J.Z.Y. Li, N. Wang, H. Li, Y. Shi, G. Guo, K. Liu, H. Zeng, Q. Zou, Therapeutic drugs targeting 2019-nCoV main protease by high-throughput screening, bioRxiv. (2020), doi:10.1101/2020.01.28.922922.
[24] Z. Xu, Y. Shi, Z. Zhu, K. Mu, X. Wang, Nelfinavir was predicted to be a potential inhibitor of 2019-nCov main protease by an integrative approach combining homology modelling, molecular docking and binding free energy calculation, BioRxiv (2020), doi:10.1101/2020.01.27.921627v1.
[25] Y. Zhou, Y. Hou, J. Shen, Y. Huang, W. Martin, F. Cheng, Network-based drug repurposing for novel coronavirus 2019-nCoV/SARS-CoV-2, Cell Discov 6 (2020) 14.
[26] D. Fiorucci, E. Milletti, F. Orofino, A. Brizzi, C. Mugnaini, F. Corelli, Computational drug repurposing for the identification of SARS-CoV-2 main protease inhibitors, J. Biomol. Struct. Dyn. (2020) 10.180/07391102.2020.1796805.
[27] M. Hagar, H. Ahmed, G. Aljohani, O. Alhaddad, Investigation of some antiviral N-heterocycles as COVID 19 drug: molecular docking and DFT calculations, Int. J. Mol. Sci. 21 (2020) 3922.
[28] J. Ortega, M. Serrano, F. Pujol, H. Rangel, Unreavealing sequence and structural features of novel coronavirus using in silico approaches: the main protease as molecular target, Excli J 19 (2020) 400.
[29] V. Alves, T. Bobrowski, C. Melo, D. Korn, S. Auerbach, C. Schmitt, E. Muratov, A. Tropsha, QSAR Modeling of SARS-CoV $M^{(pro)}$ Inhibitors Identifies Sufugolix, Cenicriviroc, Proglumetacin, and Other Drugs as Candidates for Repurposing against SARS-CoV-2, Mol. Inf. 40 (2020) 2000113.
[30] M. Smith, J.C. Smith, Repurposing Therapeutics for COVID-19: Supercomputer-Based Docking to the SARS-CoV-2 Viral Spike Protein and Viral Spike Protein-Human ACE2 Interface, ChemRxiv. Preprint. (2020), doi:10.26434/chemrxiv.11871402.v4.
[31] C. Selvaraj, D. Dinesh, U. Panwar, R. Abhirami, E. Boura, S. Singh, Structure-based virtual screening and molecular dynamics simulation of SARS-CoV-2 Guanine-N7 methyltransferase (nsp14) for identifying antiviral inhibitors against COVID-19, J. Biomol. Struct. Dyn. (2020) 10.180/07391102.2020.1778535.
[32] K. Andersen, A. Rambaut, W. Lipkin, E. Holmes, R. Garry, The proximal origin of SARS-CoV-2, Nat. Med. 26 (2020) 450.
[33] A. Bernardi, Y. Huang, B. Harris, Y. Xiong, S. Nandi, K. McDonald, R. Faller, Development and simulation of fully glycosylated molecular models of ACE2-Fc fusion proteins and their interaction with the SARS-CoV-2 spike protein binding domain, PLoS One 15 (8) (2020) e0237295, doi:10.1371/journal.pone.0237295.
[34] A. Walls, Y. Park, M. Tortorici, A. Wall, A. McGuire, D. Veesler, Structure, Function, and Antigenicity of the SARS-CoV-2 Spike Glycoprotein, Cell 181 (2020) 281.
[35] R.F.W. Bader, Quantum Theory: Atoms in Molecules, Elsevier, Toronto, 1990.
[36] M. Blanco, A. Pendas, E. Francisco, Interacting quantum atoms: A correlated energy decomposition scheme based on the Quantum Theory of Atoms in Molecules, J. Chem. Theory Comput. 1 (2005) 1096.
[37] M.O. Almeida, S.H.D.M Faria, Computational Study of the Alkylation Reaction of the Nitrogen Mustard Mechlorethamine Using NBO Model and the QTAIM Theory, Open J. Phys. Chem. 3 (2013) 127.
[38] M.O. Almeida, D. Barros, S. Araujo, S.H.D.M. Faria, V. Maltarollo, K.M. Honorio, Study on molecular structure, spectroscopic properties (FTIR and UV-Vis), NBO, QTAIM, HOMO-LUMO energies and docking studies of 5-fluorouracil, a substance used to treat cancer, Spectrochim. Acta A Mol. Biomol. Spectrosc. 184 (2017) 169.
[39] S.H.D.M. Faria, J.G. Teleschi, L. Teodoro, M.O. Almeida, Computational investigation of the carmustine (BCNU) alkylation mechanism using the QTAIM, IQA, and NBO models, Struct. Chem. (2020), doi:10.1007/s11224-020-01604-x.
[40] C.F. Matta, in: Hydrogen-hydrogen bonding: The non-electrostatic limit of closed-shell interaction between two hydrogen atoms. A critical review. Hydrogen Bonding - New Insight, (Challenges and Advances in Computational Chemistry and Physics Series), Springer Netherlands, 2006, pp. 337–376.
[41] O. Ermer, S.A. Mason, Extremely short non-bonded H-H distances in two derivatives of exo, exo-tetracyclo [6.2.$1^{3,6}$$O^{2,7}$] dodecane, J. Chem. Soc. Chem. Commun. 1 (1983) 53.
[42] B.P. Reid, M.J. O' Loughlin, R.K. Sparks, Methane-methane isotropic interaction potential from total differential cross sections, J. Chem. Phys. 83 (1985) 5656.
[43] C.F. Matta, R.F.W. Bader, An Atoms-In-Molecules study of the genetically-encoded amino acids: I. Effects of conformation and of tautomerization on geometric, atomic, and bond properties, Proteins: Struct. Funct. Genet. 40 (2000) 310.
[44] C.F. Matta, J. Hernandez-Trujillo, T. Tang, R.F.W. Bader, Cover Picture: Hydrogen-hydrogen Bonding: A Stabilizing Interaction in Molecules and Crystals, Chem. Eur. J 9 (2003) 1940.
[45] J. Hernandez-Trujillo, C.F. Matta, Hydrogen-hydrogen bonding in biphenyl revisited, Struct. Chem. 18 (2007) 849.
[46] F. Li, W. Li, M. Farzan, S. Harrison, Structure of SARS coronavirus spike receptor-binding domain complexed with receptor, Science 309 (2005) 1864.
[47] H. Berman, K. Henrick, H. Nakamura, Announcing the worldwide Protein Data Bank, Nat. Struct. Biol. 10 (2003) 980.
[48] G. Morris, R. Huey, W. Lindstrom, M. Sanner, R. Belew, D. Goodsell, A. Olson, AutoDock4 and AutoDockTools4: Automated Docking with Selective Receptor Flexibility, J. Comput. Chem. 30 (2009) 2785.
[49] E. Pettersen, T. Goddard, C. Huang, G. Couch, D. Greenblatt, E. Meng, T. Ferrin, UCSF chimera - A visualization system for exploratory research and analysis, J. Computat. Chem. 25 (2004) 1605.
[50] GaussView, Version 5.0.8 Dennington R, Keith TA, Millam JM, Semichem Inc., Shawnee Mission, KS, 2009.
[51] G.W.T. M. J. Frisch, H. B. Schlegel, G. E. Scuseria, M. A. Robb, , G.S. J. R. Cheeseman, V. Barone, G. A. Petersson, H. Nakatsuji, , M.C. X. Li, A. Marenich, J. Bloino, B. G. Janesko, R. Gomperts, , H.P.H. B. Mennucci, J. V. Ortiz, A. F. Izmaylov, J. L., D.W.-Y. Sonnenberg, F. Ding, F. Lipparini, F. Egidi, J., B.P. Goings, A. Petrone, T. Henderson, D. Ranasinghe, V. G., J.G. Zakrzewski, N. Rega, G. Zheng, W. Liang, M. Hada, M. Ehara, K., R.F. Toyota, J. Hasegawa, M. Ishida, T. Nakajima, Y. Honda, O., H.N. Kitao, T. Vreven, K. Throssell, J. A. Montgomery, Jr., J. E., F.O. Peralta, M. Bearpark, J. J. Heyd, E. Brothers, K. N. Kudin, , T.K. V. N. Staroverov, R. Kobayashi, J. Normand, K. Raghavachari, , J.C.B. A. Rendell, S. S. Iyengar, J. Tomasi, M. Cossi, J. M., M.K. Millam, C. Adamo, R. Cammi, J. W. Ochterski, R. L. Martin, K., O.F. Morokuma, J. B. Foresman, and D. J. Fox, Gaussian, Inc.: Wallingford CT, 2016.
[52] T.A. Keith, AIMAll (Version 19.02.13). TK Gristmill Software, Overland Park KS, USA, 2019 (aim.tkgristmill.com).